

# A TE-Mode Rectangular Microstrip Patch Antenna Excited by Coplanar L-Strip Feed

Matthew A. Adams and Maria Pour\*

**Abstract**—This paper proposes a coplanar L-strip feeding technique to excite the dominant transverse electric (TE) mode in a rectangular microstrip patch antenna. To excite the dominant TE<sub>10</sub> mode, the patch and ground layers are composed of artificial magnetic conductor (AMC) unit cells, and the L-strip is fashioned so that it is coplanar with the AMC patch layer. Two TE-mode microstrip patch antennas are full-wave analyzed and fabricated, one in which the AMC patch is centered with respect to the ground plane and one in which the AMC patch is shifted laterally with respect to the ground plane to improve radiation pattern symmetry. Measured results from the fabricated antennas are discussed and compared to the simulations. The proposed antennas successfully excite the dominant TE<sub>10</sub> mode while having at least 11% impedance bandwidth, 8 dBi gain, and stable broadside radiation patterns.

## 1. INTRODUCTION

Microstrip patch antennas (MPAs) are a planar type of antenna composed of a conducting patch, dielectric substrate, and conducting ground plane. Originally proposed in 1953 by Deschamps [1, 2] and practically implemented in 1972–1973 by Munson [3–5] and Howell [6], MPAs have come to the forefront of antenna technology due to their low cost, low profile, high versatility, and easy fabrication. One drawback of MPAs is that they have inherently low impedance bandwidth; however, an abundance of bandwidth enhancement methods have been proposed and studied [7–10].

To excite the transverse magnetic (TM) modes, the patch and ground plane of the MPA are made of materials that have properties similar to perfect electrical conductors (PECs); likewise, to excite the transverse electric (TE) modes, the patch and ground plane of the MPA are made of materials that have properties similar to perfect magnetic conductors (PMCs). Since PMCs do not exist naturally, artificial magnetic conductor (AMC) surfaces and electromagnetic band-gap (EBG) structures are designed and created to emulate PMCs [11]; these surfaces have very high impedance over a specified frequency range, effectively acting as a PMC or bandstop filter over that range. Some recent examples of antennas utilizing AMCs and EBG structures are given in [12–15].

Using AMC unit cells to create an MPA that excites the TE<sub>10</sub> mode was originally simulated in [16]. Another TE-mode antenna using AMC unit cells was simulated, fabricated, and measured in [17] and uses a probe with both vertical and horizontal components, termed an L-probe; the L-probe was originally used for enhancing MPA bandwidth in [10] but is also utilized to excite only the transverse components of the electric field in the presence of the AMC boundaries. It is concluded in [17] that a TE-mode patch reduces the antenna surface area required by approximately 44% when compared to a TM-mode patch made of PEC, realizing a practical reason for using TE-mode antennas over their counterparts. Successfully using an L-strip that is coplanar with a PEC patch layer to excite the TE<sub>10</sub> mode of a MPA was completed in [18]. This manuscript incorporates the contributions of

---

*Received 1 March 2023, Accepted 21 June 2023, Scheduled 9 July 2023*

\* Corresponding author: Maria Pour (maria.pour@uah.edu).

The authors are with the Department of Electrical and Computer Engineering, The University of Alabama in Huntsville, Huntsville, AL 35899, USA.

both [17] and [18] to realize a TE-mode antenna that is excited by a coplanar L-strip cutout instead of a conventional L-probe. For the proposed antenna, the feeding line is integrated within the patch layer and thus the additional layer of the L-probe feeding network required in [17] is entirely removed. This will, in turn, relax the fabrication process and reduce the overall cost. To the best of our knowledge, this is proposed for the first time for TE-mode microstrip patch antennas.

## 2. AMC UNIT CELL, AMC PATCH, AMC GROUND, AND ANTENNA CONSTRUCTION

The desired operating frequency for the proposed TE-mode antenna is 4.14 GHz. The AMC unit cell was originally designed in [19] and altered for 4–5.5 GHz operation in [17]; the reflection phase of the unit cell at 4.14 GHz is between  $\pm 45^\circ$ , so the unit cell acts as a PMC at this frequency. Therefore, no additional alterations to the unit cell in [17] had to be made. An  $8 \times 8$  AMC unit cell ground plane and  $5 \times 3$  AMC unit cell patch are created, and the individual unit cell, ground plane, and patch are depicted in Figure 1.

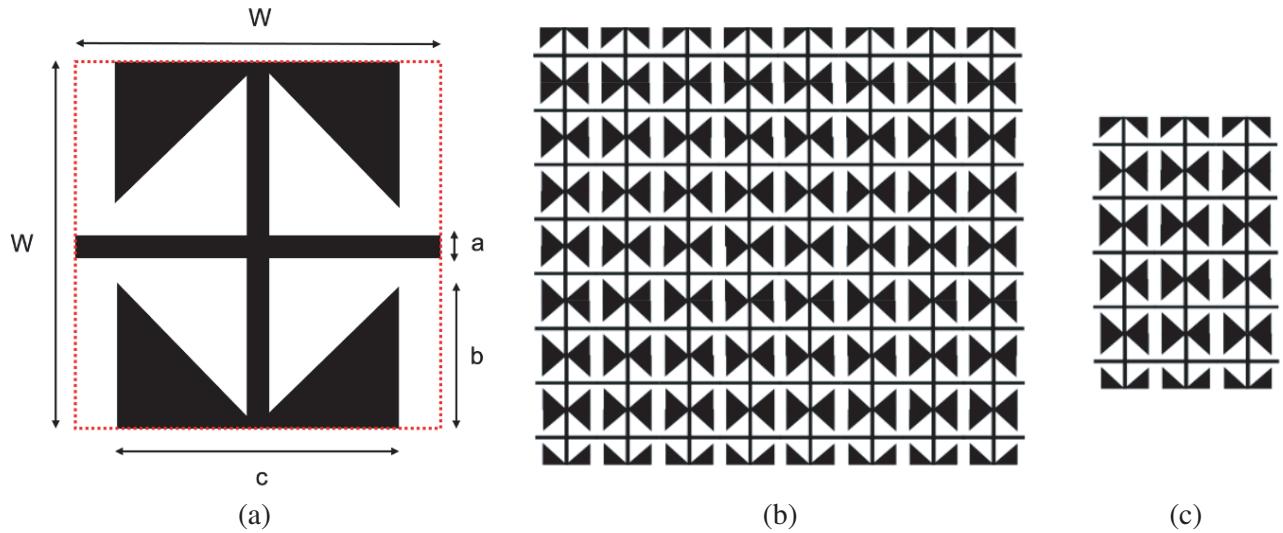


**Figure 1.** (a) Individual unit cell with dimensions  $W = 6.6$  mm,  $a = 0.2$  mm,  $b = 2.5$  mm, and  $c = 4.8$  mm, (b)  $8 \times 8$  unit cell AMC ground plane, and (c)  $5 \times 3$  unit cell AMC patch.

## 3. COPLANAR L-STRIP EXCITATION AND MICROSTRIP PATCH RADIATION

### 3.1. Antenna Construction and L-Strip Excitation

The initial TE-mode antenna, originally designed and described in [17], consists of two surfaces separated by a 3 mm air gap; each surface is composed of a solid copper ground plane layer and an AMC unit cell layer that are separated by 0.635 mm of Rogers RO3010 substrate [20] which has a dielectric constant of 10.2 and loss tangent of 0.0022 at 10 GHz. The top surface contains the AMC patch, and the bottom surface contains the AMC ground as shown in Figure 2. The two surfaces are connected via four plastic screws located at the surface corners. For the proposed antennas, the L-strip is integrated into the ground plane layer of the AMC patch as shown in Figure 2(c). L-strip integration into the unit cell layer of the AMC patch is simulated and analyzed in [21] but was not fabricated and thus, will not be discussed in this manuscript. Figure 2 depicts cross-sections of the TE-mode antennas using a conventional L-probe, an L-strip coplanar with the AMC patch unit cell layer, and an L-strip coplanar with the AMC patch ground layer.

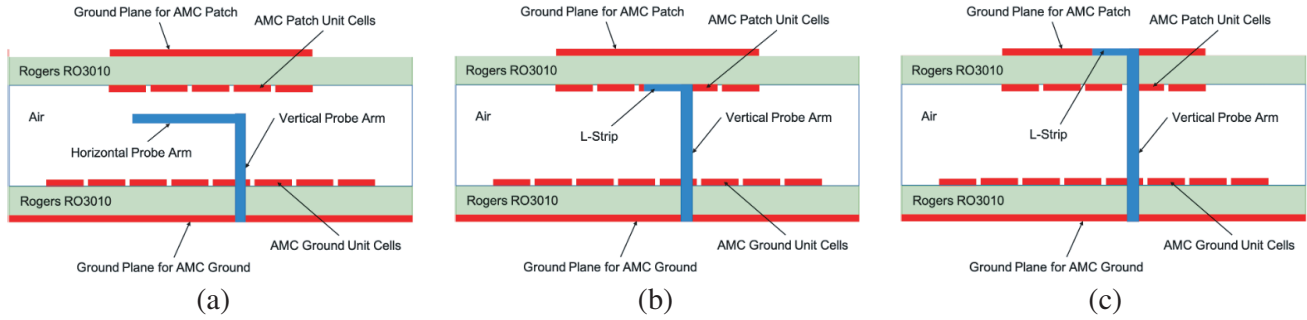


**Figure 2.** TE-mode antenna using (a) conventional L-probe, (b) L-strip integrated into the AMC patch unit cell layer, and (c) L-strip integrated into the AMC patch ground layer.

### 3.2. TE-Mode Microstrip Patch Antenna Radiation Equations

All electric and magnetic fields in a cavity must obey their respective homogeneous wave equations given by

$$\nabla^2 \mathbf{E} + k^2 \mathbf{E} = 0, \quad \nabla^2 \mathbf{H} + k^2 \mathbf{H} = 0 \quad (1)$$

where  $\mathbf{E}$  is the electric field vector,  $\mathbf{H}$  the magnetic field vector, and  $k$  the wave number. After the partial differential equations are solved using the boundary conditions, the magnetic field component in the  $z$ -direction for the general  $TE_{mn}$  mode and the dominant  $TE_{10}$  mode are given by

$$H_z = H_0 \cos\left(\frac{m\pi x}{a}\right) \cos\left(\frac{n\pi y}{b}\right) \rightarrow H_{z,m=1,n=0} = H_0 \cos\left(\frac{\pi x}{a}\right) \quad (2)$$

where  $m$  and  $n$  in general are the number of half-wave cycles along the length and width directions of the cavity, respectively. Using the microstrip patch cavity model, the radiation equations for the  $\theta$  and  $\phi$  components of the  $TE_{10}$ -mode patch are given by

$$H_{\theta,TE10} = \frac{jkbhH_0}{2\pi} \frac{e^{-jkr}}{r} e^{j(Y+Z)} \left[ \frac{\sin Y}{Y} \right] \left[ \frac{\sin Z}{Z} \right] \cos \phi \quad (3)$$

$$H_{\phi,TE10} = -\frac{jkbhH_0}{2\pi} \frac{e^{-jkr}}{r} e^{j(Y+Z)} \left[ \frac{\sin Y}{Y} \right] \left[ \frac{\sin Z}{Z} \right] \cos \theta \sin \phi \quad (4)$$

$$\text{with } X \triangleq \frac{ka}{2} \sin \theta \cos \phi, \quad Y \triangleq \frac{kb}{2} \sin \theta \sin \phi, \quad Z \triangleq \frac{kh}{2} \cos \theta \quad (5)$$

where  $a$  is the cavity length,  $b$  the cavity width, and  $h$  the cavity height.

## 4. DESIGN EVOLUTION OF THE TE-MODE MICROSTRIP PATCH USING A COPLANAR L-STRIP

The implementation of the L-strip into the AMC patch ground layer had to undergo several parametric iterations involving the vertical probe location for impedance matching, length of the horizontal L-strip, width of the L-strip cutout, length of the L-strip cutout, and the AMC patch lateral shift value. Each case is discussed in the following subsections.

### 4.1. Centered AMC Patch

Figure 3(a) depicts the corresponding  $S_{11}$  parameter curves for the parametric sweeps of the vertical probe location and the length of the horizontal L-strip, and Figure 3(b) depicts the corresponding  $S_{11}$  parameter curves for the parametric sweeps of the L-strip cutout length and L-strip cutout width. The dotted lines indicate sets of parameters that were tested, and the solid blue line indicates the set of parameters that was used in the final design, which are: a probe offset of 4.6 mm with respect to the patch center, an L-strip length of 2.9 mm, an L-strip cutout length of 4.9 mm, and an L-strip cutout width of 2.77 mm.

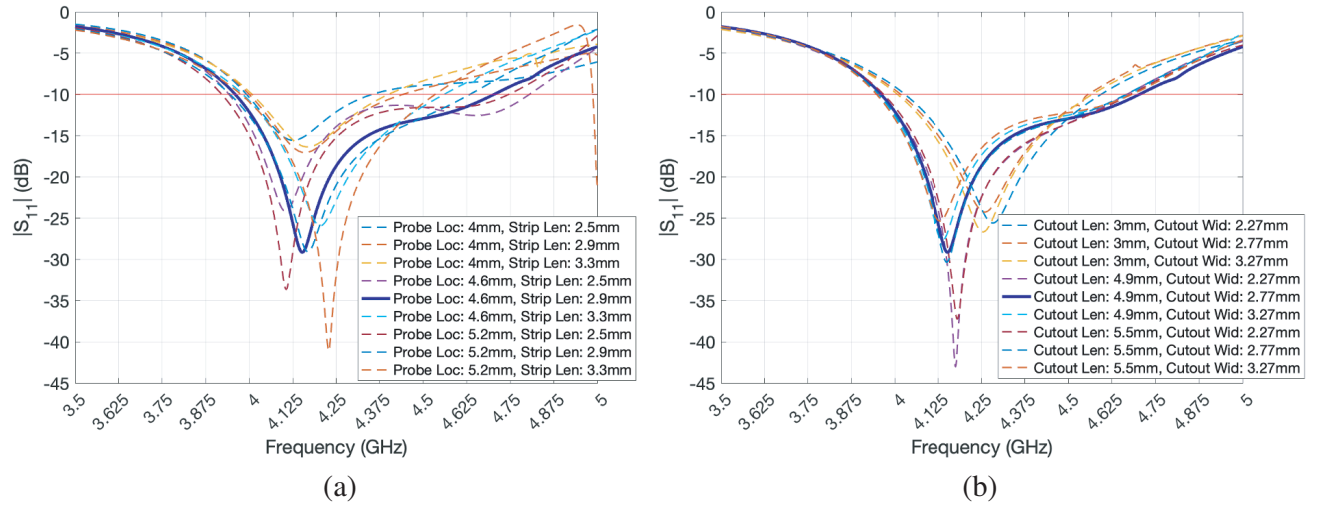


**Figure 3.** Parametric  $S_{11}$  curves varying the (a) vertical probe location and the length of the L-strip and the (b) L-strip cutout length and width for the TE-mode antenna using the centered AMC patch.

#### 4.2. Shifted AMC Patch

The AMC patch is then shifted laterally with respect to the AMC ground plane in order to improve the radiation pattern symmetry. Figure 4 depicts the corresponding  $S_{11}$  parameter curves for the parametric sweep of the AMC patch shift value as well as  $\phi = 0^\circ$ ,  $\phi = 45^\circ$ , and  $\phi = 90^\circ$  gain pattern cuts that correspond to the different AMC patch shift values of the parametric sweep; it should be noted that the gain pattern cuts for the centered AMC patch become more asymmetric as the  $\phi$  cut angle increases. The dotted lines indicate shift values that were tested, and the solid blue line indicates the shift value of 10.5 mm from the ground plane center which was used in the finalized design.

### 5. RESULTS FOR THE TE-MODE ANTENNA USING A CENTERED AMC PATCH

The AMC patch of the first antenna is centered relative to AMC ground plane; images of this antenna showing the ground layers and the AMC unit cell layers are depicted in Figure 5. The simulated and measured  $S_{11}$  curves and gain radiation pattern results are shown in Figure 6. The simulated and measured results for the proposed antenna and the antenna in [17] are tabulated in Table 1 and indicate that for the proposed antenna, the simulated broadside gain at 4.14 GHz is 8.02 dBi, and the simulated  $-10$  dB impedance bandwidth is 17.16% which corresponds to approximately 743 MHz; likewise, for the proposed antenna, the measured broadside gain at 4.14 GHz is 8.01 dBi, and the measured  $-10$  dB impedance bandwidth is 14.98% which corresponds to approximately 634 MHz. It should be noted that both measured and simulated gain pattern cuts at  $\phi = 45^\circ$  and  $\phi = 90^\circ$  in Figure 6 and Table 1 have their maximum gain values in directions offset from the broadside direction; this is caused by the introduction of the vertical probe and L-strip and is accounted for in the shifted AMC patch antenna.

Figure 6 and Table 1 indicate that the simulated and measured gain and  $S_{11}$  results for the proposed antenna are in close agreement; the main discrepancies are that the measured  $S_{11}$  curve is slightly shifted to a lower resonant frequency than the simulated, the measured  $-10$  dB impedance bandwidth is approximately 13% lower than the simulated, and measured and simulated gain values differ slightly at higher  $\phi$  gain pattern cuts due to the increasing pattern asymmetry. However, despite these discrepancies, the proposed antenna successfully excites the dominant  $TE_{10}$  mode at 4.14 GHz.

When the simulated and measured results of the proposed antenna with a centered AMC patch are compared to the results from [17], as shown in Table 1, the proposed antenna has approximately 44% higher simulated  $-10$  dB impedance bandwidth and approximately 27% higher measured  $-10$  dB impedance bandwidth; the gain radiation pattern cuts at  $\phi = 0^\circ$ ,  $\phi = 45^\circ$ , and  $\phi = 90^\circ$  of the proposed antenna are all no more than 0.6 dBi lower than those given in [17] but exhibit maximum gain values at

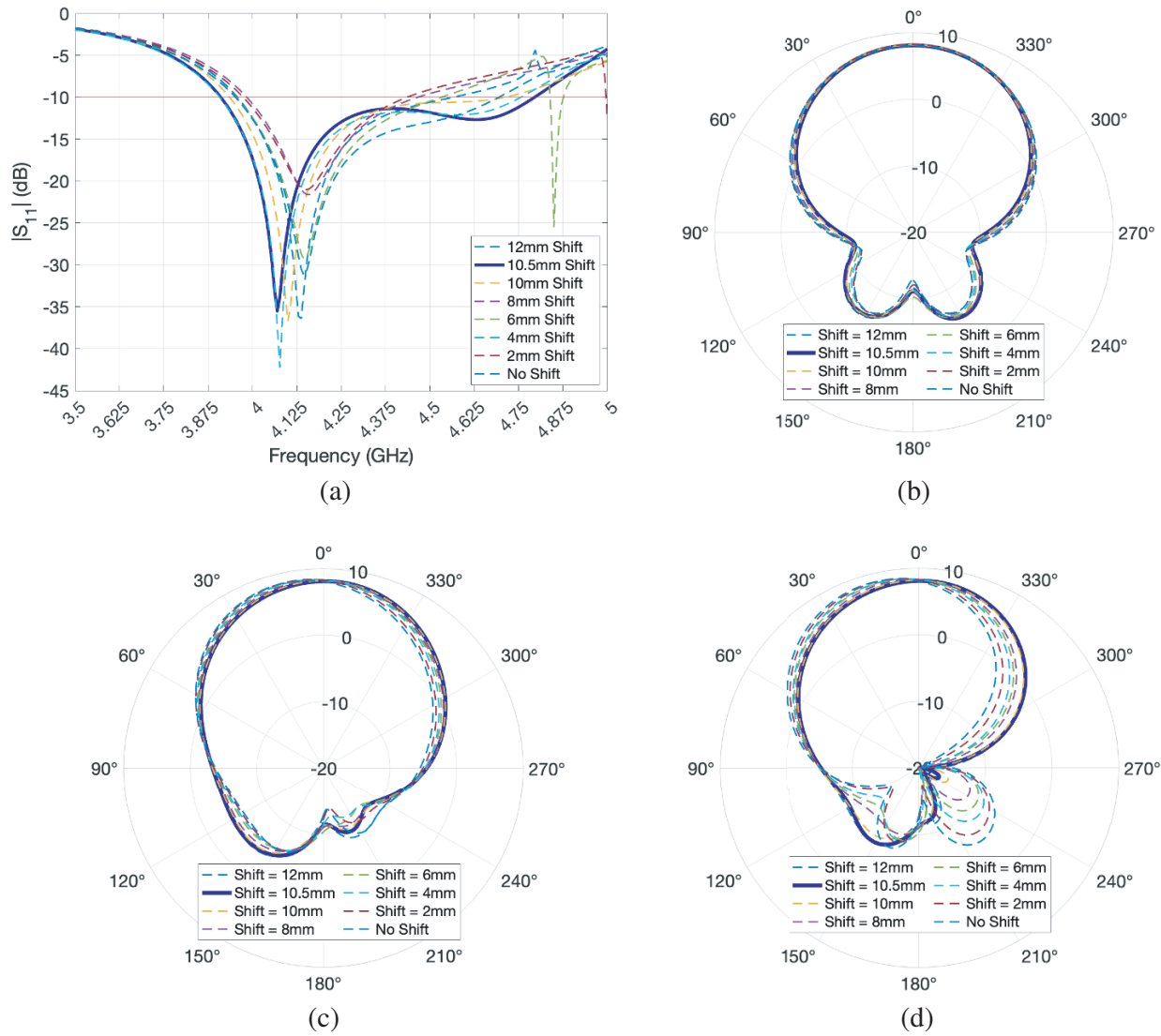


**Figure 4.** (a)  $S_{11}$  curves, (b)  $\phi = 0^\circ$  gain pattern cuts, (c)  $\phi = 45^\circ$  gain pattern cuts, and (d)  $\phi = 90^\circ$  gain pattern cuts for the parametric analysis varying the AMC patch shift value from the ground plane center.

**Table 1.** Simulated and measured results of the TE-mode antenna using a centered AMC patch compared with the simulated and measured results of the TE-mode antenna in [17].

Results Type	Center Frequency	-10 dB Impedance Bandwidth	Max Gain for $\phi = 0^\circ$ Cut, $\theta$ of Max Gain	Max Gain for $\phi = 45^\circ$ Cut, $\theta$ of Max Gain	Max Gain for $\phi = 90^\circ$ Cut, $\theta$ of Max Gain
Simulated	4.33 GHz	17.16%	8.02 dBi, $\theta = 0^\circ$	8.41 dBi, $\theta = 12^\circ$	8.68 dBi, $\theta = 14^\circ$
[17] Simulated	4.14 GHz	11.9%	8.61 dBi, $\theta = 0^\circ$	8.73 dBi, $\theta = 6^\circ$	8.83 dBi, $\theta = 8^\circ$
Measured	4.23 GHz	14.98%	8.01 dBi, $\theta = 0^\circ$	8.25 dBi, $\theta = 9^\circ$	8.43 dBi, $\theta = 12^\circ$
[17] Measured	4.21 GHz	11.8%	Not Given	Not Given	Not Given

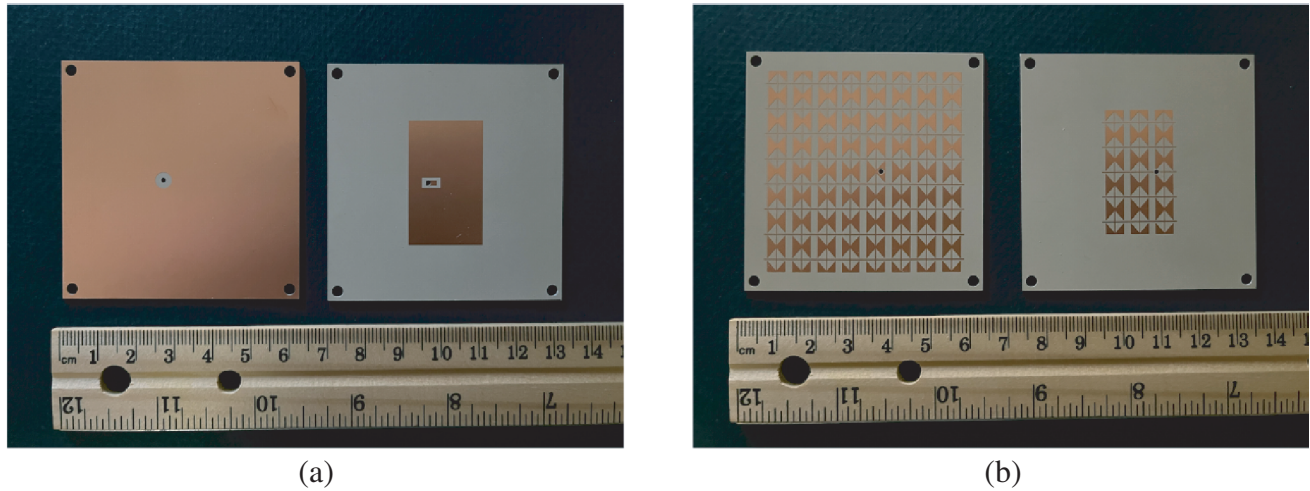


**Figure 5.** (a) Ground layers of the AMC ground and AMC patch and (b) unit cell layers of the AMC ground and AMC patch for the TE-mode antenna using a centered AMC patch.

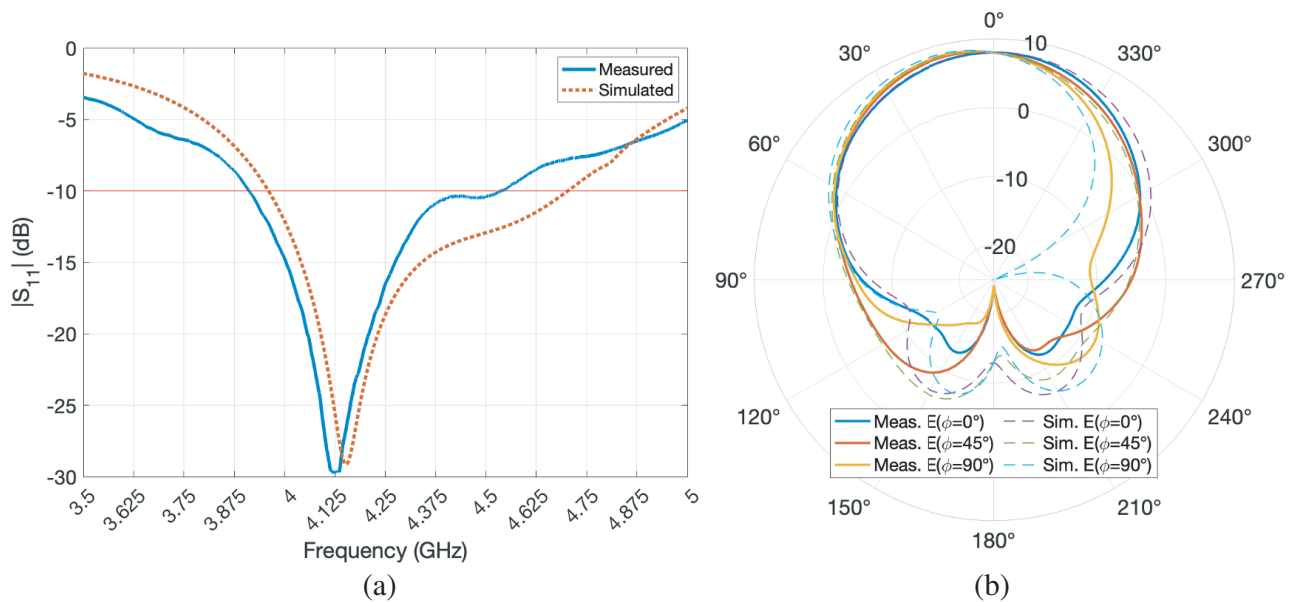


**Figure 6.** Measured and simulated (a)  $S_{11}$  curves and (b) gain radiation pattern cuts  $\phi = 0^\circ, 45^\circ, 90^\circ$  of the fabricated TE-mode antenna using a centered AMC patch at 4.14 GHz.

farther off-broadside angles. It is noted that both the proposed antenna and the antenna in [17] have increased broadside gain pattern asymmetry at increased  $\phi$  pattern cuts.

Figure 7 depicts the simulated and measured gains versus frequency of the proposed antenna, plotted over the approximate  $-10$  dB impedance bandwidth. Over the entire  $-10$  dB impedance bandwidth, the simulated and measured gains differ by no more than 2.5 dB. The simulated total antenna efficiency at the lowest frequency (3.91 GHz), the desired frequency (4.14 GHz), and the highest frequency (4.70 GHz) GHz are 87.0%, 99.8%, and 88.4%, respectively.

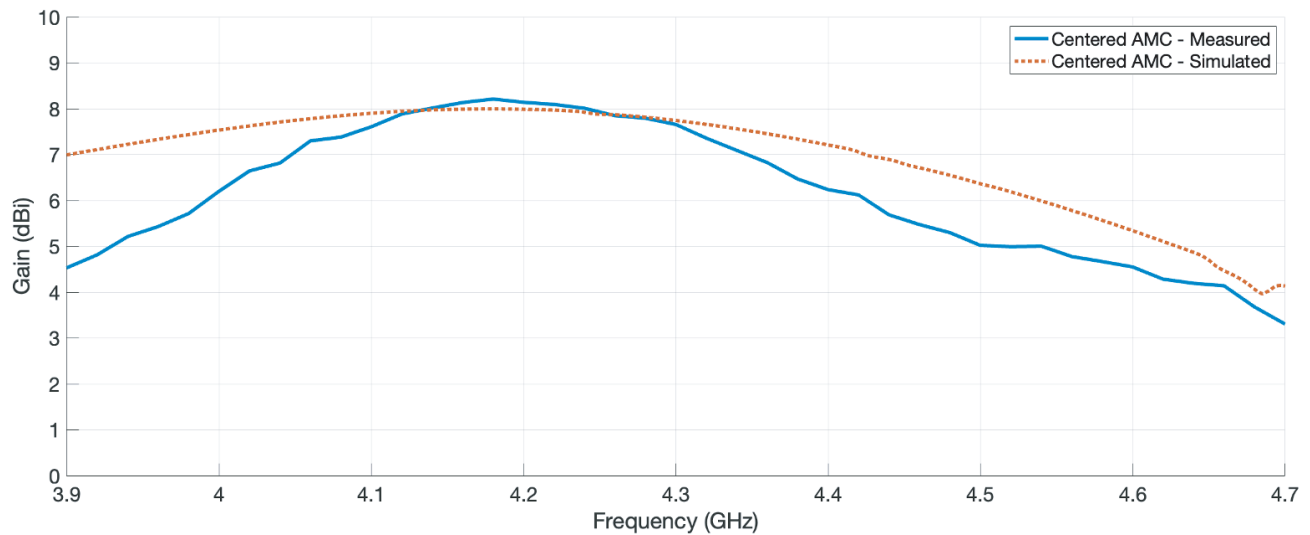


Figure 7. Simulated and measured gain versus frequency for the centered AMC patch.

### 6. RESULTS FOR THE TE-MODE ANTENNA USING A SHIFTED AMC PATCH

The AMC patch of the second antenna is shifted relative to the ground plane to account for the gain radiation pattern asymmetry depicted in Figure 6 and shown in Table 1. Using the parametric analysis detailed in Section 4.2, the patch is shifted relative to the ground plane to better match the characteristic impedance of the vertical probe and L-strip; the patch position that yielded highly desirable results was found to be 10.5 mm in the rightward direction, which is along the width dimension of the patch and is in the same direction as the probe shift for impedance matching. This location provided symmetric gain patterns about the broadside direction and a large simulated  $-10$  dB impedance bandwidth. Images of the second antenna showing the ground layers and the AMC unit cell layers are depicted in Figure 8.

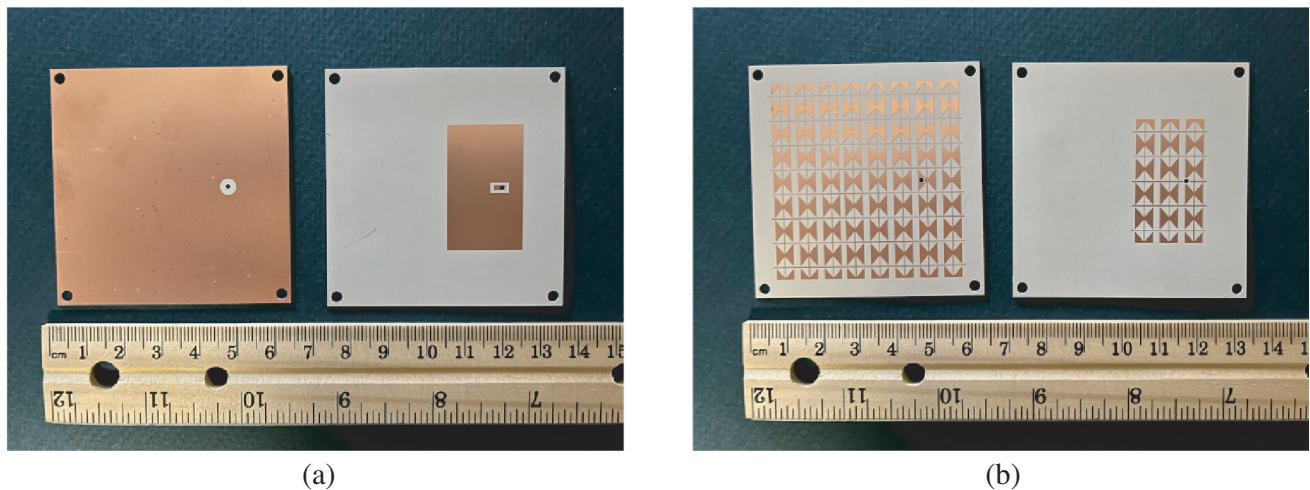
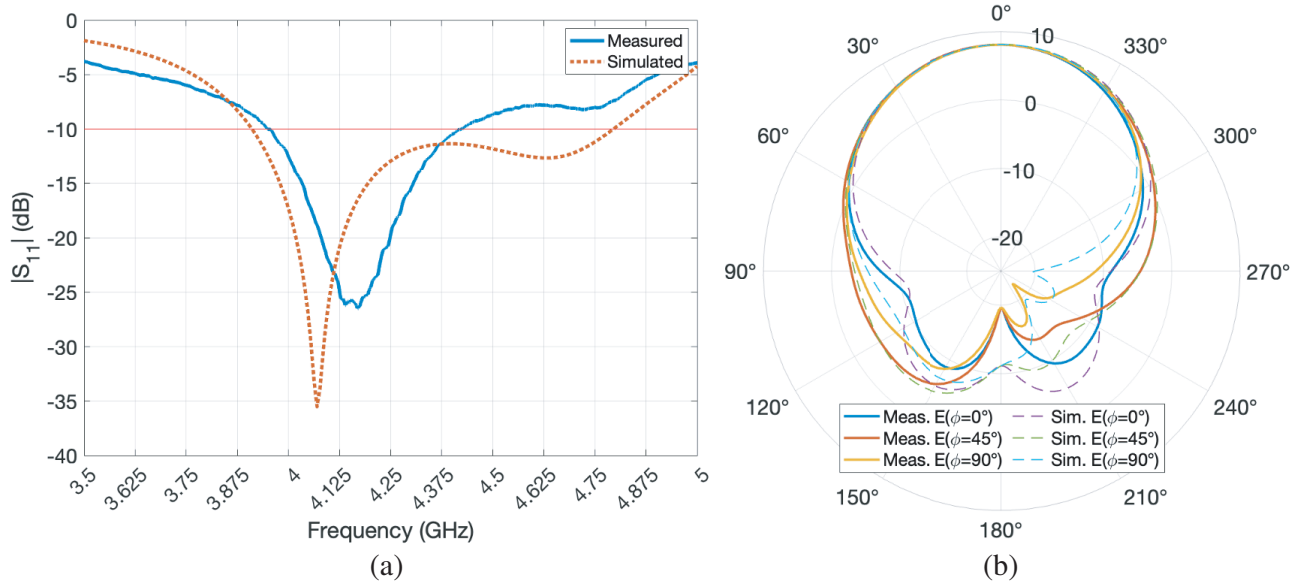


Figure 8. (a) Ground layers of the AMC ground and AMC patch and (b) unit cell layers of the AMC ground and AMC patch for the TE-mode antenna using a shifted AMC patch.

The simulated and measured gain radiation patterns and  $S_{11}$  results are shown in Figure 9. The simulated and measured results of the proposed antenna and the antenna in [17] are tabulated in Table 2 and show that for the proposed antenna, the simulated broadside gain at 4.14 GHz is 8.11 dBi, and



**Figure 9.** Measured and simulated (a)  $S_{11}$  curves and (b) gain radiation pattern cuts  $\phi = 0^\circ, 45^\circ, 90^\circ$  for the fabricated TE-mode antenna using a shifted AMC patch at 4.14 GHz.

**Table 2.** Simulated and measured results of the proposed TE-mode antenna using a shifted AMC patch compared with the simulated and measured results of the TE-mode antenna in [17].

Results Type	Center Frequency	-10 dB Impedance Bandwidth	Max Gain for $\phi = 0^\circ$ Cut, $\theta$ of Max Gain	Max Gain for $\phi = 45^\circ$ Cut, $\theta$ of Max Gain	Max Gain for $\phi = 90^\circ$ Cut, $\theta$ of Max Gain
Simulated	4.35 GHz	20.17%	8.11 dBi, $\theta = 0^\circ$	8.11 dBi, $\theta = -2^\circ$	8.11 dBi, $\theta = -2^\circ$
[17] Simulated	4.14 GHz	11.9%	8.61 dBi, $\theta = 0^\circ$	8.73 dBi, $\theta = 6^\circ$	8.83 dBi, $\theta = 8^\circ$
Measured	4.19 GHz	11.29%	8.07 dBi, $\theta = 0^\circ$	8.07 dBi, $\theta = 0^\circ$	8.07 dBi, $\theta = 0^\circ$
[17] Measured	4.21 GHz	11.8%	Not Given	Not Given	Not Given

the simulated  $-10$  dB impedance bandwidth is 20.1% which corresponds to approximately 877 MHz; likewise, for the proposed antenna, the measured broadside gain at 4.14 GHz is 8.07 dBi and, the measured  $-10$  dB impedance bandwidth is 11.29% which corresponds to approximately 473 MHz. The measured  $-10$  dB impedance bandwidth is 56% less than the simulated bandwidth; it should be noted that a large portion of the simulated  $S_{11}$  curve is very near the  $-10$  dB impedance bandwidth cutoff, thus, a slight increase in the measured  $S_{11}$  values relative to the simulated  $S_{11}$  values of this region could negate a large percentage of the bandwidth determined by the simulation. This measured bandwidth discrepancy is likely attributed to the solder joints, potential misalignment of the two layers due to the manual assembly of the board, and unwanted reflections from the connecting cable for testing.

The simulated maximum gain for the  $\phi = 0^\circ$ ,  $\phi = 45^\circ$ , and  $\phi = 90^\circ$  radiation pattern cuts are all at a constant 8.11 dBi and are all no more than  $2^\circ$  off the boresight direction ( $\theta = 0^\circ$ ); likewise, the measured maximum gain for the  $\phi = 0^\circ$ ,  $\phi = 45^\circ$ , and  $\phi = 90^\circ$  radiation pattern cuts are all 8.07 dBi and are all exactly along the boresight direction. The simulated and measured maximum gain values occurring at or near boresight indicate that the lateral shift was successful in accounting for the radiation pattern asymmetry introduced in the first antenna and the antenna in [17].

When the simulated and measured results of the proposed antenna with a shifted AMC patch are compared to the results from [17], as shown in Table 2, the proposed antenna has approximately 71% higher simulated  $-10$  dB impedance bandwidth but approximately 4% lower measured  $-10$  dB

impedance bandwidth; the gain radiation pattern cuts at  $\phi = 0^\circ$ ,  $\phi = 45^\circ$ , and  $\phi = 90^\circ$  of the proposed antenna are no more than 0.72 dBi lower than those given in [17] and exhibit a maximum gain value of no more than 2 degrees off-broadside, showing a significant improvement compared to [17] and the proposed TE-mode antenna using a centered AMC patch.

Figure 10 depicts the simulated and measured gains versus frequency of the proposed antenna, plotted over the approximate  $-10$  dB impedance bandwidth. Over the entire  $-10$  dB impedance bandwidth, the simulated and measured gains differ by no more than 1.6 dB. The total antenna efficiency at the lowest frequency (3.91 GHz), the desired frequency (4.14 GHz), and the highest frequency (4.81 GHz) GHz are 90.0%, 98.4%, and 88.8%, respectively.

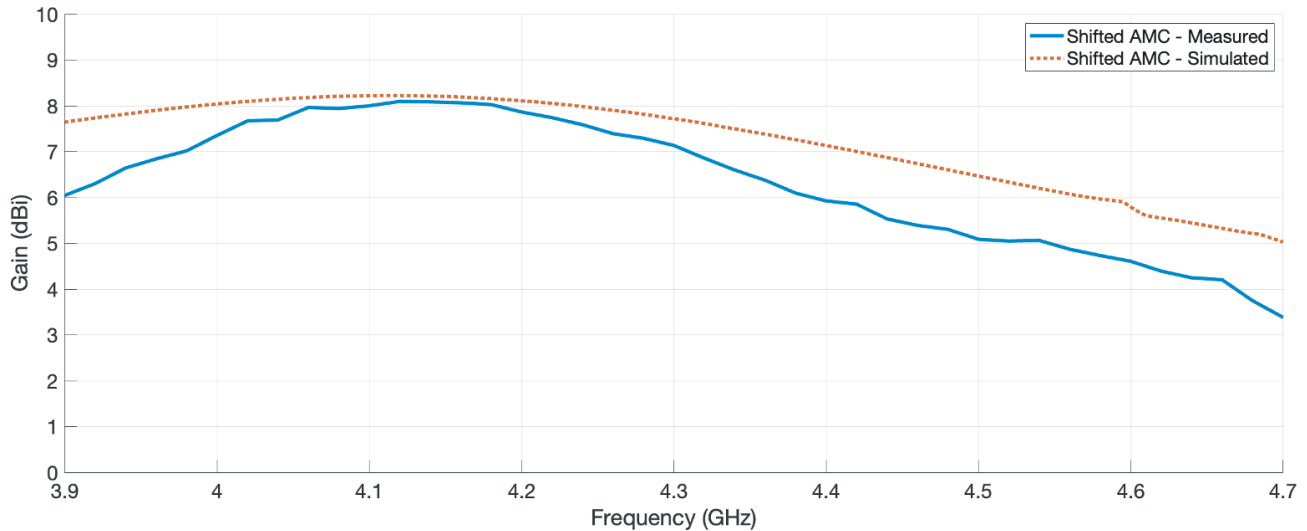


**Figure 10.** Simulated and measured gain versus frequency for the shifted AMC patch.

## 7. CONCLUSION

Two novel TE-mode antennas using AMC patches are proposed, simulated, manufactured, and tested; each antenna is excited by an L-strip that is coplanar with the ground layer of the AMC patch. The first antenna has the AMC patch centered above the ground plane, and the second antenna has the AMC patch shifted laterally with respect to the ground plane. The simulated and measured results of the first antenna are in close agreement and indicate that incorporating the L-strip into the ground layer of the AMC patch successfully excites the dominant  $TE_{10}$  mode of the antenna, thus, successfully replacing the L-probe feeding method of [17] to allow for easier fabrication and lower overall cost. Furthermore, the second antenna shows that shifting the AMC patch laterally with respect to the ground plane successfully reduces the broadside asymmetry of the  $\phi = 45^\circ$  and  $\phi = 90^\circ$  gain radiation pattern cuts of the antenna. The measured results in each case were in close agreement with the simulated results, barring the  $-10$  dB impedance bandwidth measurement of the shifted AMC patch case in which an explanation of the discrepancy is given. The results of the proposed antennas are compared to the results of the antenna in [17], and it is shown that the proposed antenna has either similar or better performance than that given in [17]. Overall, the proposed TE-mode antennas with coplanar L-strip excitation successfully excite the  $TE_{10}$  mode with greater than 11% impedance bandwidth, at least 8 dBi of gain, and symmetric gain radiation patterns about the broadside direction.

## REFERENCES

1. Deschamps, G. A. and W. Sichak, "Microstrip microwave antennas," *Proc. of Third Symp. on USAF Antenna Research and Development Program*, October 18–22, 1953.

2. Deschamps, G. A., "Theoretical aspects of microstrip waveguides," *IEEE Transactions on Microwave Theory and Techniques*, Vol. 2, No. 1, 100–102, 1954.
3. Munson, R. E., "Microstrip phased array antennas," *Proc. of Twenty-Second Symp. on USAF Antenna Research and Development Program*, October 1972.
4. Munson, R. E., "Conformal microstrip antennas and microstrip phased arrays," *IEEE Transactions on Antennas and Propagation*, Vol. 22, No. 1, 74–78, January 1974.
5. Munson, R. E. and J. K. Krutsinger, "Single slot cavity antennas assembly," January 23, 1973.
6. Howell, J., "Microstrip antennas," *IEEE Transactions on Antennas and Propagation*, Vol. 23, No. 1, 90–93, 1975.
7. Derneryd, A. G. and I. Karlsson, "Broadband microstrip antenna element and array," *IEEE Transactions on Antennas and Propagation*, Vol. 29, No. 1, January 1981.
8. Sabban, A., "A new broadband stacked two-layer microstrip antenna," *IEEE Antenna Propagat. Soc. Int. Symp. Digest*, 63–66, 1983.
9. Huynh, T. and K.-F. Lee, "Single-layer single-patch wideband microstrip antenna," *Electronics Letters*, Vol. 34, 1442–1443, 1998.
10. Luk, K. M., C. L. Mak, Y. L. Chow, and K. F. Lee, "Broadband microstrip patch antenna," *Electronics Letters*, Vol. 34, 1442–1443, 1998.
11. Balanis, C. A., *Advanced Engineering Electromagnetics*, 2nd Edition, J. Wiley & Sons, Hoboken, NJ, 2012.
12. Han, T., X.-Y. Cao, J. Gao, Y.-L. Zhao, and Y. Zhao, "A coding metasurface with properties of absorption and diffusion for RCS reduction," *Progress In Electromagnetics Research C*, Vol. 75, 181–191, 2017.
13. Islam, M. T. and M. S. Alam, "Compact EBG structure for alleviating mutual coupling between patch antenna array elements," *Progress In Electromagnetics Research*, Vol. 137, 425–438, 2013.
14. Mol, V. A. L. and C. K. Aanandan, "Wideband radar cross section reduction using artificial magnetic conductor checkerboard surface," *Progress In Electromagnetics Research M*, Vol. 69, 171–183, 2018.
15. Yin, B., M. Ye, Y. Yu, and J. Gu, "A dual-band, miniaturized, AMC-based wearable antenna for health monitoring applications," *Progress In Electromagnetics Research C*, Vol. 112, 165–177, 2021.
16. Yang, S.-L. S., A. A. Kishk, and K.-F. Lee, "Rectangular patch Antenna supported by artificial magnetic conducting surface," *2008 URSI General Assembly Chicago*, August 2008.
17. Mitha, T. and M. Pour, "Investigation of dominant transverse electric mode in microstrip patch antennas," *IEEE Transactions on Antennas and Propagation*, Vol. 67, No. 1, 643–648, 2019.
18. Radavaram, S. and M. Pour, "A wideband coplanar L-strip fed rectangular patch antenna," *IEEE Antennas and Wireless Propagation Letters*, Vol. 20, No. 9, 1779–1783, 2021.
19. Yang, S.-L. S., A. A. Kishk, and K.-F. Lee, "The forbidden bandgap characteristic of EBG structures," *Microw. Opt. Technol. Lett.*, Vol. 50, No. 11, 2965–2967, 2008.
20. RO3000 Series Circuit Materials RO3003 RO3006 RO3010 and RO3035 High Frequency Laminates, Rogers Corp., Chandler, AZ, USA, 2022.
21. Adams, M., "Excitation of the dominant transverse electric mode of a microstrip patch antenna using a coplanar L-strip feeding technique," Master's Thesis, Dept. of Electrical and Computer Engineering, The University of Alabama in Huntsville, Huntsville, AL, ProQuest, 2022.